bioRxiv preprint doi: https://doi.org/10.1101/169516; this version posted July 28, 2017. The copyright holder for this preprint (which was not certified by peer review) is the author/funder, who has granted bioRxiv a license to display the preprint in perpetuity. It is made available under aCC-BY 4.0 International license.

1 **Chemical Gating of the Mechanosensitive Piezo1 Channel by Asymmetric Binding of its**
2 **Agonist Yoda1**
3

4 Jerome J. Lacroix*[1], Wesley M. Botello-Smith[2] and Yun Luo[2]
5
6 [1]Graduate College of Biomedical Sciences, Western University of Health Sciences, 309 E.
7 Second St, Pomona, CA 91766
8 [2]College of Pharmacy, Western University of Health Sciences, 309 E. Second St, Pomona, CA
9 91766
10
11
12 ***corresponding author:**
13 Dr. Jerome Lacroix
14 Western University of Health Sciences
15 309 E. Second St, Pomona, CA 91766
16 Tel: 909-469-8201
17 Email: jlacroix@westernu.edu
18
19
20
21
22
23

bioRxiv preprint doi: https://doi.org/10.1101/169516; this version posted July 28, 2017. The copyright holder for this preprint (which was not certified by peer review) is the author/funder, who has granted bioRxiv a license to display the preprint in perpetuity. It is made available under aCC-BY 4.0 International license.

24 **Abstract**

25 Piezo proteins are homotrimeric ion channels that play major roles in normal and pathological
26 mechanotransduction signaling in mammalian organisms. Their pharmacological control hence
27 represents a potential therapeutic avenue. Yoda1, a Piezo1-selective small molecule agonist, is
28 the only known selective Piezo modulator. How Yoda1 selectively interacts with Piezo1 and
29 opens its pore is unknown. Here, by engineering and characterizing chimeras, we identified a
30 minimal region responsible for Yoda1 binding. This region is located at the interface between the
31 pore and the putative mechanosensory domains in each subunit. By characterizing hybrid
32 channels containing Yoda1-insensitive and Yoda1-sensitive monomers, we demonstrate that the
33 presence of only one Yoda1-sensitive Piezo1 subunit is sufficient for chemical activation,
34 implicating that the asymmetric binding of Yoda1 to a single subunit enables channel opening.
35 These findings shed light onto the gating mechanisms of Piezo channels and will pave the way
36 for the rationale design of new Piezo channels modulators.

37

bioRxiv preprint doi: https://doi.org/10.1101/169516; this version posted July 28, 2017. The copyright holder for this preprint (which was not certified by peer review) is the author/funder, who has granted bioRxiv a license to display the preprint in perpetuity. It is made available under aCC-BY 4.0 International license.

38 **Introduction**

39 Piezo proteins are very large (~1MDa) trimeric mechanosensitive ion channels (Fig 1a) which
40 transduce various forms of mechanical stimuli such as shear stress and membrane stretch into
41 important biological signals. In mammals, only two Piezo isoforms named Piezo1-2 have been
42 identified. In spite of their recent discovery, these isoforms have been implicated in a
43 bewildering number of mechanotransduction processes including touch sensation(1-3),
44 proprioception(4), hearing(5), vascular(6, 7) and brain development(8), blood flow sensing(9),
45 osmotic homeostasis(10) and epithelium regulation(11, 12). Both gain-of-functions and loss-of-
46 functions Piezo mutations are associated with human diseases such as xerocytosis(13, 14, 10,
47 15), arthrogryposis(16-22) and lymphedema(23). Recent studies suggest Piezo channels may also
48 play important roles in other conditions such as sleep apnea(24) and visceral pain(25).

49 An avenue to treat these diseases would be to correct Piezo channel activity with small
50 molecule agonists and/or antagonists. On the other hand, the availability of selective Piezo
51 modulators would allow us to precisely determine the contribution of each Piezo isoform to
52 complex physiological functions. Unfortunately, the current pharmacology of Piezo channels is
53 extremely limited, with a single Piezo1-selective small molecule agonist named Yoda1(26) (Fig
54 1b) and no known isoform-selective inhibitors. Hence, understanding how Yoda1 selectively
55 binds and activates Piezo1 is a key step to rationally design new small molecule modulators with
56 high selectivity.

57 Yoda1 was recently identified using a simultaneous high-throughput agonist screening on
58 both Piezo1 and 2 isoforms. Although Piezo2 shares more than 65% of its primary amino acid
59 sequence with Piezo1, Yoda1 possesses strict Piezo1 selectivity with no measurable modulatory
60 effects on Piezo2 activity. The activation of Piezo1 by Yoda1 originates from the binding of

bioRxiv preprint doi: https://doi.org/10.1101/169516; this version posted July 28, 2017. The copyright holder for this preprint (which was not certified by peer review) is the author/funder, who has granted bioRxiv a license to display the preprint in perpetuity. It is made available under aCC-BY 4.0 International license.

61 Yoda1 to one or more unknown binding site(s) on the Piezo1 channel(26). Based on these
62 observations, we have generated Piezo1-Piezo2 chimeras to identify a minimal protein region
63 responsible for Yoda1 binding selectivity. By characterizing hybrid channels containing wild-
64 type (WT) and Yoda1-insensitive Piezo1 subunits, we further show that the binding of Yoda1 to
65 a single subunit is sufficient for activation of the trimeric channel.
66
67

bioRxiv preprint doi: https://doi.org/10.1101/169516; this version posted July 28, 2017. The copyright holder for this preprint (which was not certified by peer review) is the author/funder, who has granted bioRxiv a license to display the preprint in perpetuity. It is made available under aCC-BY 4.0 International license.

68 **Results**

69 **Molecular determinants for Yoda1 selectivity**

70 The purified Piezo1 channel reconstituted in artificial bilayer remains Yoda1-sensitive(26).
71 Hence, the Piezo1 protein possesses an endogenous agonist Yoda1 binding site that enables
72 channel activation. The strict Piezo1-selectivity exhibited by Yoda1 must then originate from
73 amino acid differences between the Piezo1 and Piezo2 primary sequence. Since chimeras
74 between evolutionary-distant Piezo homologs remain functional(27), we reasoned that chimeras
75 between mouse Piezo1 (mPiezo1) and mouse Piezo2 (mPiezo2) will yield functioning proteins
76 with altered Yoda1-sensitivity. Since Yoda1 stabilize the open pore conformation in absence of
77 mechanical stimulation(26), we reasoned that the Yoda1 binding site is likely located near the
78 pore in the C-terminal region. We thus designed three C-terminal chimeras and named them by
79 the residue number after which the C-terminal sequence is from mPiezo2 (i.e. Ch1961, Ch2063
80 and Ch2456, Fig 1c and Supplementary Fig 1). The C-terminal chimeras were expressed into
81 HEK293T cells and characterized using a fluorescence assay based on the calcium-sensitive
82 organic dye Fluo8-AM (Fig 1d). A variant of this assay was previously used to characterize
83 Yoda1 sensitivity of Piezo homologs and disease variants(26). The chimeras Ch2063 and 2456
84 exhibit concentration-dependent fluorescence responses similar to WT mPiezo1 (Fig 1e). In
85 contrast, Ch1961 was totally insensitive to Yoda1 in the range of concentrations tested, similar to
86 the Yoda1-insensitive mPiezo2. We independently confirmed the ability of the three C-terminal
87 chimeras to respond to mechanical stimulation induced by an acute hypotonic shock, a simple
88 way to experimentally activate Piezo channels. All chimeras displayed robust responses similar
89 to mPiezo1. These responses were significantly larger than the response obtained from cells
90 transfected with a control vector (Fig 1f).

bioRxiv preprint doi: https://doi.org/10.1101/169516; this version posted July 28, 2017. The copyright holder for this preprint (which was not certified by peer review) is the author/funder, who has granted bioRxiv a license to display the preprint in perpetuity. It is made available under aCC-BY 4.0 International license.

91

92 **A minimal region for Yoda1 binding**

93 To verify that the region 1961-2063 contains the molecular determinants for Yoda1 binding, we
94 created the internal chimera Ch1961-2063. We next divided this region into three sub-regions
95 (region 1: 1961-2004, region 2: 2005-2034 and region 3: 2035-2063) and engineered every
96 possible combination of "sub-chimeras" replacing one or two sub-regions by the corresponding
97 sequence from the mPiezo2 homolog (Fig 2a and Supplementary Fig 1).

98 For simplicity, these sub-chimeras were named by the number of the sub-region(s) being
99 replaced (e.g. Ch1+3 in Fig 2a replaces the sub-regions 1961-2004 and 2035-2063 by their
100 homolog sequences from mPiezo2). To reduce fluorescence background, calcium-sensitive
101 fluorescence was measured by co-transcriptionally expressing the genetically-encoded
102 fluorescent indicator GCaMP6m (see Methods). Wide-field fluorescence live-cell imaging
103 showing GCaMP6m time course upon Yoda1 application in the presence or absence of mPiezo1
104 can be seen in Video1 and Video2, respectively. The fluorescence of GCaMP6m does not change
105 upon Yoda1 application in absence of mPiezo1, as when using Fluo8-AM (Fig 1d). All tested
106 sub-chimeras displayed diminished fluorescence responses compared to mPiezo1 (Fig 2b). Yet,
107 none of them completely suppressed the fluorescence response as seen in cells transfected with
108 mPiezo2 or with the internal chimera 1961-2063. The internal chimera 1961-2063 remains able
109 to elicit robust fluorescence responses upon acute hypotonic chock (Fig 2c) and to produce
110 mechano-dependent ionic currents with amplitude similar to wild type mPiezo1 (Fig 2d). This
111 shows that the elimination of the fluorescence signal in cells transfected with Ch1961-2063
112 originates from the loss of the agonist binding site rather than a loss of channel function. We next

bioRxiv preprint doi: https://doi.org/10.1101/169516; this version posted July 28, 2017. The copyright holder for this preprint (which was not certified by peer review) is the author/funder, who has granted bioRxiv a license to display the preprint in perpetuity. It is made available under aCC-BY 4.0 International license.

113 fitted the plots of the normalized peak currents I/I_{max} against the pulse pressure P (Fig 2e) with a
114 standard two-state Boltzmann equation:

$$\frac{I}{I_{max}} = \frac{1}{1 + e^{-k(P-P_0)}}$$

115 with P_0 the pressure corresponding to $I = I_{max}/2$ and k a constant representing the intrinsic
116 electromechanical coupling of the channel. The fits yielded $P_0 = 32.29 \pm 0.93$ mmHg for WT
117 mPiezo1, consistent with previous studies(26). However, the chimera Ch1961-2063 exhibits an
118 increased threshold for mechanosensitivity with a fitted P_0 value of 56.43 ± 0.76 mmHg (see
119 Supplementary Table 1).

120

121 **Minimal Yoda1-sensitive subunit stoichiometry for Yoda1-mediated activation**

122 The presence of the entire mPiezo1 1961-2063 region appears necessary for chemical activation
123 with Yoda1. Interestingly, this region is strategically located at the interface between the pore
124 and the blade in each subunit (Fig 1a and Fig 2f). Since this region exists in each of the three
125 Piezo1 subunits, Yoda1 could potentially bind to each subunit. How many subunits need to
126 interact with the Yoda1 agonist to open the channel's pore?

127 In our assay, the measured fluorescence F is a function of the saturation function ν of the
128 protein P by the ligand L and of the background fluorescence q:

$$F = q + b_{max} \times \nu \; (1)$$

129 At t = 0 s, [Yoda1] = 0 µM, then ν =o:

$$\frac{F - F_0}{F_0} = \frac{(q + b_{max} \times \nu) - q}{q} = \frac{b_{max}}{q} \times \nu = B_{max}\nu \quad (2)$$

130 In case of multiple binding sites per protein, the saturation function equals the total
131 concentrations of bound ligands ($[L]_{bound}$) over the total concentration of protein ($[P]_0$):

bioRxiv preprint doi: https://doi.org/10.1101/169516; this version posted July 28, 2017. The copyright holder for this preprint (which was not certified by peer review) is the author/funder, who has granted bioRxiv a license to display the preprint in perpetuity. It is made available under aCC-BY 4.0 International license.

$$\mathbf{\nu} = \frac{[\mathbf{L}]_{\mathbf{bound}}}{[\mathbf{P}]_{\mathbf{0}}} \quad (3)$$

132 Assuming the existence of three identical and independent Yoda1 binding sites:

$$\frac{[\mathbf{L}]_{\mathbf{bound}}}{[\mathbf{P}]_{\mathbf{0}}} = \frac{[\mathbf{PL}] + 2[\mathbf{PL}] + 3[\mathbf{PL}]}{[\mathbf{P}] + [\mathbf{PL}] + [\mathbf{PL}] + [\mathbf{PL}]} \quad (4)$$

133 The different protein species are related by the corresponding macroscopic dissociation constant

134 K_1, K_2 and K_3 corresponding to each binding step:

$$\mathbf{K_1} = \frac{[\mathbf{P}][\mathbf{L}]}{[\mathbf{PL}]} \; ; \; \mathbf{K_2} = \frac{[\mathbf{PL}][\mathbf{L}]}{[\mathbf{PL_2}]} \; ; \; \mathbf{K_3} = \frac{[\mathbf{PL_2}][\mathbf{L}]}{[\mathbf{PL_3}]}$$

135 By replacing the macroscopic constants:

$$\mathbf{\nu} = \frac{\frac{[\mathbf{L}]}{\mathbf{K_1}} + \frac{2[\mathbf{L}]}{\mathbf{K_1K_2}} + \frac{3[\mathbf{L}]}{\mathbf{K_1K_2K_3}}}{1 + \frac{[\mathbf{L}]}{\mathbf{K_1}} + \frac{[\mathbf{L}]}{\mathbf{K_1K_2}} + \frac{[\mathbf{L}]}{\mathbf{K_1K_2K_3}}} \quad (5)$$

136 The macroscopic constants are related to the microscopic dissociation constant K_d by the number

137 or possible binding combinations $\Omega_{n,i}$ for each binding step i and for n binding sites:

$$\mathbf{K_i} = \frac{\mathbf{\Omega_{n,i-1}}}{\mathbf{\Omega_{n,i}}} \times \mathbf{K_d} = \frac{\binom{\mathbf{n}}{\mathbf{i-1}}}{\binom{\mathbf{n}}{\mathbf{i}}} = \frac{\mathbf{i}}{\mathbf{n - i + 1}} \times \mathbf{K_d}$$

138 Replacing the macroscopic constants by the K_d gives:

$$\mathbf{\nu} = \frac{\frac{3[\mathbf{L}]}{\mathbf{K_d}} + \frac{6[\mathbf{L}]^2}{\mathbf{K_d}^2} + \frac{3[\mathbf{L}]^3}{\mathbf{K_d}^3}}{1 + \frac{3[\mathbf{L}]}{\mathbf{K_d}} + \frac{3[\mathbf{L}]^2}{\mathbf{K_d}^2} + \frac{[\mathbf{L}]^3}{\mathbf{K_d}^3}} \quad (6)$$

139 Equation (6) further simplifies by applying a binomial reduction:

$$\mathbf{\nu} = \frac{\mathbf{n}[\mathbf{L}]}{\mathbf{K_d} + [\mathbf{L}]} \quad (7)$$

bioRxiv preprint doi: https://doi.org/10.1101/169516; this version posted July 28, 2017. The copyright holder for this preprint (which was not certified by peer review) is the author/funder, who has granted bioRxiv a license to display the preprint in perpetuity. It is made available under aCC-BY 4.0 International license.

140 The details about this reduction can be found elsewhere(28). Assuming the binding of one or
141 more ligand per channel produces similar channel opening, every bound species in the numerator
142 of equation (6) contribute proportionally to the observed fluorescence signal:

$$\frac{F - F_0}{F_0} = B_{max} \times \frac{n[L]}{K_d + [L]} \quad (8)$$

143 However, if the binding of two or three ligands is required for channel activation, the fraction of
144 channel with a single ligand does not contribute to the signal. In this case, the fluorescence signal
145 follows:

$$\frac{F - F_0}{F_0} = B_{max} \times \frac{\frac{6[L]^2}{{K_d}^2} + \frac{3[L]^3}{{K_d}^3}}{1 + \frac{3[L]}{K_d} + \frac{3[L]^2}{{K_d}^2} + \frac{[L]^3}{{K_d}^3}} \quad (9)$$

146 Similarly, if the binding of three ligands is necessary for channel activation, the fluorescence
147 signal follows:

$$\frac{F - F_0}{F_0} = B_{max} \times \frac{\frac{3[L]^3}{{K_d}^3}}{1 + \frac{3[L]}{K_d} + \frac{3[L]^2}{{K_d}^2} + \frac{[L]^3}{{K_d}^3}} \quad (10)$$

148 We tested these three binding situations modeled by equations (8), (9) and (10) by performing a
149 dose-response on WT mPiezo1 with more data points (Fig 3a). Curve fitting clearly shows that a
150 model with 3 ligands per channel (equation (10)) or with more than 2 ligands (equation (9)) does
151 not fit well the data (Fig 3a and Table 1). In contrast, a model where every bound species equally
152 contribute to the signal (equation (8)) provides a better fit. This suggests the binding of Yoda1 to
153 a single binding site in one subunit is sufficient for channel opening. As indicated previously, the
154 reported Kd values obtained from curve fitting are not accurate estimates of the dissociation
155 constant due to the poor aqueous solubility of Yoda1 above 20-30 μM(26).

bioRxiv preprint doi: https://doi.org/10.1101/169516; this version posted July 28, 2017. The copyright holder for this preprint (which was not certified by peer review) is the author/funder, who has granted bioRxiv a license to display the preprint in perpetuity. It is made available under aCC-BY 4.0 International license.

156 **Table 1: Fitting results for different binding stoichiometry**

Number of ligand per trimeric channel	1-3	2-3	3
Model equation	(8)	(9)	(10)
B_{max}	1.701 ± 0.152	1.155 ± 0.097	0.744 ± 0.102
K_d (μM)	11.990 ± 1.941	2.245 ± 0.297	1.110 ± 0.103
R^2	0.964	0.812	0.825

157

158 To further investigate the minimal binding stoichiometry of Yoda1, we co-expressed WT
159 mPiezo1 subunits with Yoda1-insensitive Ch1961-2063 subunits by transfecting HEK293T cells
160 with different ratios of the corresponding plasmids. The subunit mixtures lead to four channel
161 species with a number of WT subunits ranging from 0 to 3 (Fig 3b). Assuming WT and chimeric
162 subunits are expressed in proportion to the amount of transfected plasmid and assuming hybrid
163 channels are formed by random association of WT and chimeric subunits, the fraction (Fr) of
164 assembled channels with *i* WT subunits for a trimeric channels is given by the equation:

$$\mathbf{Fr_{(i)}} = \binom{3}{i} \mathbf{f_{Ch}^{(3-i)} f_{WT}^{i}} \quad (11)$$

165 With f_{Ch} and f_{WT} the relative fractions of plasmids encoding chimeric and WT subunits,
166 respectively.

167 We transfected HEK293T cells with different plasmid mixtures containing 10%, 30%,
168 50% or 100% WT mPiezo1. The predicted fraction for each species and for each tested mixture
169 is indicated in Fig 3b. Surprisingly, cells transfected with a mixture containing only 10% WT
170 subunits produced robust fluorescence signals (Fig 3c). Indeed, at saturating Yoda
171 concentrations, this signal amounts to approximately a third of the fluorescence signal observed
172 in cells transfected with 100% WT plasmids. When mixing 10% WT subunit with 90% chimeric
173 subunit, the predicted fraction of channels containing three WT subunits is only 0.1%, while the
174 large majority of WT subunits exist in channels containing two chimeric subunits (Fig 3b). This

bioRxiv preprint doi: https://doi.org/10.1101/169516; this version posted July 28, 2017. The copyright holder for this preprint (which was not certified by peer review) is the author/funder, who has granted bioRxiv a license to display the preprint in perpetuity. It is made available under aCC-BY 4.0 International license.

175 indicates that the presence of a single WT subunit is sufficient for chemical activation of the
176 channel with Yoda1. This observation is consistent with the fitting results from Fig 3a.
177 Next, we further performed a global fit of the dose-responses obtained for different
178 mixtures and for WT mPiezo1. Based on equations (8) and (11), the fluorescence signal from a
179 heterogeneous population of channel species with i number of WT subunit(s) will be a function
180 of the saturation fraction multiplied by the total relative fraction of channel species contributing
181 to the signal (i.e. having one or more WT subunit):

$$\frac{\mathbf{F-F_0}}{\mathbf{F_0}} = \mathbf{B_{max}}\left(\frac{\mathbf{[L]}}{\mathbf{[L]+Kd}}\right)\left(\mathbf{Fr_{(i=3)}} + \mathbf{F_{r(i=2)}} + \mathbf{Fr_{(i=1)}}\right)$$

182 Since $\sum_{i=0}^{3} \mathbf{Fr_{(i)}} = \mathbf{1}$, the equation can be simplified:

$$\frac{\mathbf{F-F_0}}{\mathbf{F_0}} = \mathbf{B_{max}}\left(\frac{\mathbf{[L]}}{\mathbf{[L]+Kd}}\right)\left(\mathbf{1} - \mathbf{Fr_{(i=0)}}\right) \quad \mathbf{(12)}$$

183 Where $Fr_{(i=0)}$ correspond to the non-contributing fraction of channels containing three chimeric
184 subunits. Equation (12) was used for a global fit of the data shown in Fig 3c. The fitting was
185 done with only two shared fitted parameters, B_{max} and K_d, while the fractions Fr_0 were calculated
186 for each tested plasmid mixture. The global fit produced an overall coefficient of determination
187 R^2 of 0.907, a B_{max} value of 4.219 ± 0.325 and a K_d of 9.624 ± 1.412 μM. This fitted K_d value is
188 similar to the K_d value obtained by fitting the WT dose-response with the binding model
189 corresponding to equation (8) (11.990 ± 1.941 μM, see Fig 3 and Table 1). Differences in the
190 fitted B_{max} can be due to fluctuations in background fluorescence q between experiments as
191 indicated by equations (1) and (2).
192 Another way of confirming that each channel containing at least one WT subunit is able
193 to open in response to Yoda1 binding is to compare the observed vs. predicted contributing
194 fractions of Yoda1-sensitive hybrid channels. From equation (12) we can see that:

bioRxiv preprint doi: https://doi.org/10.1101/169516; this version posted July 28, 2017. The copyright holder for this preprint (which was not certified by peer review) is the author/funder, who has granted bioRxiv a license to display the preprint in perpetuity. It is made available under aCC-BY 4.0 International license.

$$\frac{\frac{\Delta F}{F_0}(\text{mix})}{\frac{\Delta F}{F_0}(\text{WT})} = \left(1 - Fr_{0(\text{mix})}\right) \quad (13)$$

195 With $\Delta F/F_{0(mix)}$ the fluorescence signal observed when mixing WT and chimeric subunits,
196 $\Delta F/F_{0(WT)}$ the fluorescence signal observed for WT channels and $1\text{-}Fr_{0(mix)}$ the observed
197 contributing fraction of channels obtained when mixing subunits in a given ratio. We determined
198 the observed contributing fraction ($1\text{-}Fr_{0(mix)}$) by calculating the term on the left of equation (13)
199 for each Ch:WT ratio. This number was averaged from six Yoda1 concentrations ranging
200 between 2 μM and 75 μM. The observed contributing fractions were then plotted against the
201 predicted contributing fractions of hybrid channels containing more than one ($1 \leq i \leq 3$), more
202 than 2 ($2 \leq i \leq 3$) or 3 WT subunits ($i = 3$) using equation (11). The plots shows that the observed
203 fractions nearly perfectly match the predicted fractions only if hybrid channels containing one or
204 more WT subunits contribute to the fluorescence signal (Fig 3d, dotted magenta line).
205
206

bioRxiv preprint doi: https://doi.org/10.1101/169516; this version posted July 28, 2017. The copyright holder for this preprint (which was not certified by peer review) is the author/funder, who has granted bioRxiv a license to display the preprint in perpetuity. It is made available under aCC-BY 4.0 International license.

207 **Discussion**

208 In this study, we created chimeras between Piezo1 and Piezo2 to identify the minimal region
209 required for the selective binding of the agonist Yoda1. In principle, the Yoda1 binding site on
210 Piezo1 could be directly identified by solving the structure of the agonist-channel complex.
211 However, the current resolution of the mPiezo1 structure (4.8Å) is too low to resolve most side
212 chains in the protein. This would preclude the localization of the 21-atom Yoda1 molecule. On
213 the other hand, the agonist binding site could be identified in functioning Piezo1 channels using a
214 spectroscopic nanopositioning approach(29). However, such spectroscopic measurements would
215 require fluorescent versions of Yoda1 which retain the same pharmacological properties.

216 Our data show that the strict selectivity of Yoda1 towards mPiezo1 originates from a
217 minimal protein region spanning residues 1961 to 2063. This region contains 17 residues that are
218 not conserved between the two mammalian Piezo isoforms and that are dispersed into three
219 clusters (Supplementary Fig 1). The mPiezo1 channel becomes fully insensitive to Yoda1 only
220 when all three clusters are exchanged with their counterpart from the mPiezo2 primary sequence.
221 Any chimeric combination made by exchanging two out of three clusters yielded chimeras with
222 some degree of Yoda1 sensitivity (Fig 2b). Thus, some, if not all, residues from each cluster are
223 required to form the Yoda1 binding site. We do not know yet whether Yoda1 directly interacts
224 with these residues or whether some of these residues are required to form a binding site in a
225 nearby region. Hence, we envisage two hypotheses to explain the origin of Yoda1 isoform-
226 selectivity. First, Yoda1 may directly interact with Piezo1-specific residues. In this case, Yoda1
227 must directly interact with some of the identified residues in each cluster in the region 1961-
228 2063. Second, Yoda1 may directly interact with residues that are conserved in Piezo1 and Piezo2
229 but whose conformation depends on the presence of non-conserved residues in each cluster in the
230 1961-2063 region. In this case the selectivity of Yoda1 must originate from a difference in the

bioRxiv preprint doi: https://doi.org/10.1101/169516; this version posted July 28, 2017. The copyright holder for this preprint (which was not certified by peer review) is the author/funder, who has granted bioRxiv a license to display the preprint in perpetuity. It is made available under aCC-BY 4.0 International license.

231 conformation of the binding site rather than from a difference in the chemical composition of its
232 residues. Future studies will be needed to distinguish between these two possibilities.
233 Activation of the Yoda1-insensitive Ch1961-2063 chimera by negative pressure in a cell-
234 attached patch requires higher pressures than WT mPiezo1 channels (Fig 2e). Incidentally, the
235 threshold for mechanical activation of mPiezo2 channels is also higher than for mPiezo1(26).
236 Hence, the region identified here as necessary for agonist binding appears as an important region
237 to regulate the mechanical sensitivity of Piezo channels.
238 The predicted fractions of hybrid channels obtained by mixing WT and mutant subunits
239 are true if only two assumptions are satisfied. The first is that the cellular expression of both
240 subunits is proportional to the quantity of transfected plasmid. This seems to be the case
241 according to the similar level of ionic current measured in cells transfected with the individual
242 plasmids (Fig 2d). The other assumption is that both subunits randomly assemble to form
243 trimeric channels. We do not know if this is the case. Protein-protein interaction experiments
244 such as resonance energy transfer between fluorescent probes covalently linked to WT and
245 chimeric subunits would confirm the existence of hybrid channels. However, the absolute
246 quantification of the species in a heterogenous population of hybrid channels would be
247 technically challenging to assess.
248 The fact that a single WT subunit suffices to confer Yoda1 sensitivity to the trimeric
249 channel has profound mechanistic consequences regarding the gating process of the channel.
250 Homo-multimeric ion channels with a central permeation pathway often undergo symmetrical
251 concerted conformational rearrangements in all subunits to control the opening/closure of their
252 pore. Hence, binding of Yoda1 to one subunit may induce a concerted transition in all subunits in
253 the pore region that stabilizes the channel's open state. On the other hand, Yoda1 binding in a

bioRxiv preprint doi: https://doi.org/10.1101/169516; this version posted July 28, 2017. The copyright holder for this preprint (which was not certified by peer review) is the author/funder, who has granted bioRxiv a license to display the preprint in perpetuity. It is made available under aCC-BY 4.0 International license.

254 single subunit could induce partial opening of the pore. In this case, incremental binding of the
255 ligand in each subunit would yield distinct open states with incremental sub-conductance levels.
256 These hypotheses could be tested by recording single channel currents from concatenated Piezo
257 channels made by fusing a known number of WT and chimeric subunits in the same open
258 reading frame. However, the large size of a single mammalian Piezo subunit (2400-2600 amino
259 acids) would make those experiments challenging.
260
261 In summary, we have identified the minimal binding region of the only known isoform selective
262 modulator of the mechanosensitive Piezo ion channel family. We further show that the binding
263 of the agonist to only one subunit enables ligand-induced activation of the trimeric channel. This
264 study shed lights on the gating mechanisms of Piezo proteins and will pave the way for the
265 rationale design of small molecules with relevant pharmacological properties.
266

bioRxiv preprint doi: https://doi.org/10.1101/169516; this version posted July 28, 2017. The copyright holder for this preprint (which was not certified by peer review) is the author/funder, who has granted bioRxiv a license to display the preprint in perpetuity. It is made available under aCC-BY 4.0 International license.

267 **Materials and Methods**

268 *Molecular Cloning:* A pCDNA3 plasmid containing mPiezo1 was obtained from Dr. Mikhail
269 Shapiro (Caltech) and was originally a gift from Dr. Patapoutian (The Scripps Research
270 Institute). A Sport6 plasmid encoding mPiezo2 was directly obtained from Dr. Pataouptian. To
271 create the polycistronic vector pCDNA3-mPZ1-IRES-GCaMP6m, we PCR-amplified the
272 pCDNA-mPZ1 plasmid, the internal ribosome entry site (IRES) cassette from a pIRES-eGFP
273 plasmid and the GCaMP6m cDNA from a pGP-CMV-GCaMP6m plasmid (Addgene plasmid
274 #40754) and assembled them using the NEBuilder HiFi DNA Assembly kit (New England
275 Biolabs). A similar procedure was used to create pCDNA3-mPZ2-IRES-GCaMP6m, pCDNA3-
276 GCaMP6m and the empty control vector pCDNA3. All mPZ1-mPZ2 chimeras with or withouth
277 the IRES-GCaMP6m cassette were created using the same approach. All constructs were verified
278 by automated Sanger sequencing (Genewiz).

279

280 *Cell culture and transfection:* HEK293T cells (a gift from Dr. Mikhail Shapiro and originally
281 purchased directly from ATCC) were cultured in standard conditions (37°C, 5% CO_2) in a
282 DMEM medium supplemented with Penicillin (100 U/mL), streptomycin (0.1 mg/mL), 10%
283 sterile Fetal Bovine Serum and 1X MEM non-essential amino-acid without L-glutamine. All cell
284 culture products were purchased from Sigma-Aldrich. Transfection was done on cells with a
285 passage number lower than 25 using polyethylenimine (PEI, Polysciences #23966). Briefly, a
286 sterile mixture of DNA:PEI (1:4 w/w) was prepared using sterile 100mM NaCl solution and
287 added directly to the cell's culture medium (220ng of total DNA was added per cm^2 of cultured
288 surface). Culture medium was changed 16-20 hours after transfection. For fluorescence
289 experiments, cells seeded on clear-bottom black 96-well plates (Nunc) were transfected at ~50%

bioRxiv preprint doi: https://doi.org/10.1101/169516; this version posted July 28, 2017. The copyright holder for this preprint (which was not certified by peer review) is the author/funder, who has granted bioRxiv a license to display the preprint in perpetuity. It is made available under aCC-BY 4.0 International license.

290 confluence 2-4 days before the experiment. For electrophysiology experiments, cells seeded on
291 uncoated coverslips were transfected at ~10% confluence 1 day prior recordings.
292
293 *Calcium imaging, osmotic shocks and chemical treatment:* Fluo-8 AM was purchased from
294 abcam (ab142773), dissolved in dimethyl sulfoxide (DMSO) and stored in 5mM aliquots at -
295 20°C. Yoda1 was purchased from Sigma-Aldrich (#SML1558), dissolved in DMSO and stored
296 in 10mM aliquots at -20°C. For experiments with Fluo8-AM, cells were washed with a normal
297 physiological solution (NPSS) containing 140mM NaCl, 5mM KCl, 2mM $MgCl_2$, 1mM $CaCl_2$,
298 10mM HEPES (pH 7.4 with HCl or NaOH) and 10mM Glucose and incubated for 1 hour in a
299 37°C/5% CO_2 incubator with a NPSS solution containing 3-5 μM Fluo-8 AM. After incubation,
300 cells were washed again with 100μL NPSS and placed on a Nikon inverted fluorescence
301 microscope. Epifluorescence excitation was provided by a 100W mercury lamp through a 20X
302 objective and fluorescence images were obtained using a standard GFP filter set and acquired at
303 1 frame/sec using a Nikon Digital Sight camera and the Nikon Digital Element D software.
304 During recordings, 100μL of a 2X Yoda1 NPSS solution was added to the cells at t = 30 s or
305 sometimes at t = 10 s. Total DMSO concentration was kept below 1% for all tested Yoda
306 concentrations. For osmotic shocks, 200μL of a hypotonic solution was added to the 100μL
307 isotonic NPSS during the recording. Hypotonic solution was similar to NPSS except the NaCl
308 concentration was reduced from 140mM to 5mM. For experiments with GCaMP6m,
309 fluorescence imaging was done similarly except the 1 hour Fluo-8 AM treatment was replaced
310 by a 1 hour NPSS incubation. Fluorescence images were analyzed with ImageJ.
311

bioRxiv preprint doi: https://doi.org/10.1101/169516; this version posted July 28, 2017. The copyright holder for this preprint (which was not certified by peer review) is the author/funder, who has granted bioRxiv a license to display the preprint in perpetuity. It is made available under aCC-BY 4.0 International license.

312 *Cell-attached patch-clamp recordings:* During recordings, the membrane potential was zeroed
313 using a depolarizing bath solution containing 140 mM KCl, 1mM $MgCl_2$, 10 mM glucose and 10
314 mM HEPES pH 7.3 (with KOH). Fire-polished patch pipettes with a diameter of 1-5 µm and
315 resistance of 1-5 MΩ were filled with a recording solution containing 130 mM NaCl, 5 mM KCl,
316 1 mM $CaCl_2$, 1 mM $MgCl_2$, 10 mM TEA-Cl and 10 mM HEPES pH 7.3 (with NaOH). Stretch-
317 activated currents were recorded in the cell-attached configuration after seal formation using a
318 Multiclamp 700B amplifier (Axon) and a high-speed pressure clamp (HSPC-1, ALA Scientific
319 Instruments). The membrane potential inside the patch was held at -80mV. Data were recorded at
320 a sampling frequency of 10 kHz and filtered offline at 2 kHz using pClamp (Axon). Although the
321 data shown are unaltered traces, peak current amplitudes were determined by adjusting the
322 baseline at the end of the pressure pulse. No mechanosensitive ionic currents could be detected in
323 these conditions in untransfected HEK293T cells (n = 25, data not shown).
324
325 *Statistics:* For imaging, each experiment was done in duplicate and repeated n times (n values are
326 indicated in the figures). For each experiment, the fluorescence intensity taken from 30 cells (15
327 cells per image stack in duplicate) was averaged. Cells were selected randomly for analysis at the
328 beginning of the movie before Yoda1 application. Dead cells with abnormal shape or unusual
329 high fluorescence (i.e. high cytosolic $[Ca^{2+}]$) were excluded from analyses. The final $F_{(t=1min)}$-
330 F_0/F_0 values and standard errors were calculated by averaging the mean values from n
331 experiment. For electrophysiology, the relative peak current values and standard error (Fig 2e)
332 are from averaging one series of recordings from n transfected cells. To test statistical difference
333 between two mean values, we performed 2-tails unpaired Student's t tests. The exact t-values and

bioRxiv preprint doi: https://doi.org/10.1101/169516; this version posted July 28, 2017. The copyright holder for this preprint (which was not certified by peer review) is the author/funder, who has granted bioRxiv a license to display the preprint in perpetuity. It is made available under aCC-BY 4.0 International license.

334 standard p-value ranges are indicated in each figure. The degree of freedom equals n-1. All
335 fitting were done using OriginPro 2017.
336

bioRxiv preprint doi: https://doi.org/10.1101/169516; this version posted July 28, 2017. The copyright holder for this preprint (which was not certified by peer review) is the author/funder, who has granted bioRxiv a license to display the preprint in perpetuity. It is made available under aCC-BY 4.0 International license.

337 **Acknowledgment**

338 We thank Dr. Xiaoning Bi for lending us an inverted fluorescence microscope, Dr. Mikhail
339 Shapiro from lending us a Multiclamp 700B amplifier and Dr. Ardem Patapoutian for the gift of
340 the mPiezo cDNAs. We also thank David Kent, John T. Fly and Brennan Kidder for their
341 technical help with molecular biology.

342

343

344

345

346

bioRxiv preprint doi: https://doi.org/10.1101/169516; this version posted July 28, 2017. The copyright holder for this preprint (which was not certified by peer review) is the author/funder, who has granted bioRxiv a license to display the preprint in perpetuity. It is made available under aCC-BY 4.0 International license.

347 **References**

348 1. Coste B, Mathur J, Schmidt M, Earley T J, Ranade S, Petrus M J, Dubin A E, Patapoutian
349 A. 2010. Piezo1 and Piezo2 are essential components of distinct mechanically activated
350 cation channels. Science 330;55-60. doi: 10.1126/science.1193270.
351 2. Coste B, Xiao B, Santos J S, Syeda R, Grandl J, Spencer K S, Kim S E, Schmidt M,
352 Mathur J, Dubin A E, Montal M, Patapoutian A. 2012. Piezo proteins are pore-forming
353 subunits of mechanically activated channels. Nature 483;176-181. doi:
354 10.1038/nature10812.
355 3. Ranade S S, Woo S H, Dubin A E, Moshourab R A, Wetzel C, Petrus M, Mathur J,
356 Begay V, Coste B, Mainquist J, Wilson A J, Francisco A G, Reddy K, Qiu Z, Wood J N,
357 Lewin G R, Patapoutian A. 2014. Piezo2 is the major transducer of mechanical forces for
358 touch sensation in mice. Nature 516;121-125. doi: 10.1038/nature13980.
359 4. Woo S H, Lukacs V, de Nooij J C, Zaytseva D, Criddle C R, Francisco A, Jessell T M,
360 Wilkinson K A, Patapoutian A. 2015. Piezo2 is the principal mechanotransduction
361 channel for proprioception. Nature neuroscience 18;1756-1762. doi: 10.1038/nn.4162.
362 5. Wu Z, Grillet N, Zhao B, Cunningham C, Harkins-Perry S, Coste B, Ranade S, Zebarjadi
363 N, Beurg M, Fettiplace R, Patapoutian A, Muller U. 2016. Mechanosensory hair cells
364 express two molecularly distinct mechanotransduction channels. Nature neuroscience
365 doi: 10.1038/nn.4449.
366 6. Ranade S S, Qiu Z, Woo S H, Hur S S, Murthy S E, Cahalan S M, Xu J, Mathur J,
367 Bandell M, Coste B, Li Y S, Chien S, Patapoutian A. 2014. Piezo1, a mechanically
368 activated ion channel, is required for vascular development in mice. Proceedings of the
369 National Academy of Sciences of the United States of America 111;10347-10352. doi:
370 10.1073/pnas.1409233111.
371 7. Li J, Hou B, Tumova S, Muraki K, Bruns A, Ludlow M J, Sedo A, Hyman A J,
372 McKeown L, Young R S, Yuldasheva N Y, Majeed Y, Wilson L A, Rode B, Bailey M A,
373 Kim H R, Fu Z, Carter D A, Bilton J, Imrie H et al. 2014. Piezo1 integration of vascular
374 architecture with physiological force. Nature 515;279-282. doi: 10.1038/nature13701.
375 8. Pathak M M, Nourse J L, Tran T, Hwe J, Arulmoli J, Le D T, Bernardis E, Flanagan L A,
376 Tombola F. 2014. Stretch-activated ion channel Piezo1 directs lineage choice in human
377 neural stem cells. Proceedings of the National Academy of Sciences of the United States
378 of America 111;16148-16153. doi: 10.1073/pnas.1409802111.
379 9. Wang S, Chennupati R, Kaur H, Iring A, Wettschureck N, Offermanns S. 2016.
380 Endothelial cation channel PIEZO1 controls blood pressure by mediating flow-induced
381 ATP release. The Journal of clinical investigation 126;4527-4536. doi:
382 10.1172/JCI87343.
383 10. Cahalan S M, Lukacs V, Ranade S S, Chien S, Bandell M, Patapoutian A. 2015. Piezo1
384 links mechanical forces to red blood cell volume. eLife 4doi: 10.7554/eLife.07370.
385 11. Eisenhoffer G T, Loftus P D, Yoshigi M, Otsuna H, Chien C B, Morcos P A, Rosenblatt
386 J. 2012. Crowding induces live cell extrusion to maintain homeostatic cell numbers in
387 epithelia. Nature 484;546-549. doi: 10.1038/nature10999.
388 12. Gudipaty S A, Lindblom J, Loftus P D, Redd M J, Edes K, Davey C F, Krishnegowda V,
389 Rosenblatt J. 2017. Mechanical stretch triggers rapid epithelial cell division through
390 Piezo1. Nature 543;118-121. doi: 10.1038/nature21407.

bioRxiv preprint doi: https://doi.org/10.1101/169516; this version posted July 28, 2017. The copyright holder for this preprint (which was not certified by peer review) is the author/funder, who has granted bioRxiv a license to display the preprint in perpetuity. It is made available under aCC-BY 4.0 International license.

391 13. Demolombe S, Duprat F, Honore E, Patel A. 2013. Slower Piezo1 inactivation in
392 dehydrated hereditary stomatocytosis (xerocytosis). Biophysical journal 105;833-834.
393 doi: 10.1016/j.bpj.2013.07.018.
394 14. Andolfo I, Alper S L, De Franceschi L, Auriemma C, Russo R, De Falco L, Vallefuoco
395 F, Esposito M R, Vandorpe D H, Shmukler B E, Narayan R, Montanaro D, D'Armiento
396 M, Vetro A, Limongelli I, Zuffardi O, Glader B E, Schrier S L, Brugnara C, Stewart G W
397 et al. 2013. Multiple clinical forms of dehydrated hereditary stomatocytosis arise from
398 mutations in PIEZO1. Blood 121;3925-3935, S3921-3912. doi: 10.1182/blood-2013-02-
399 482489.
400 15. Andolfo I, Russo R, Manna F, Shmukler B E, Gambale A, Vitiello G, De Rosa G,
401 Brugnara C, Alper S L, Snyder L M, Iolascon A. 2015. Novel Gardos channel mutations
402 linked to dehydrated hereditary stomatocytosis (xerocytosis). American journal of
403 hematology 90;921-926. doi: 10.1002/ajh.24117.
404 16. Coste B, Houge G, Murray M F, Stitziel N, Bandell M, Giovanni M A, Philippakis A,
405 Hoischen A, Riemer G, Steen U, Steen V M, Mathur J, Cox J, Lebo M, Rehm H, Weiss S
406 T, Wood J N, Maas R L, Sunyaev S R, Patapoutian A. 2013. Gain-of-function mutations
407 in the mechanically activated ion channel PIEZO2 cause a subtype of Distal
408 Arthrogryposis. Proceedings of the National Academy of Sciences of the United States of
409 America 110;4667-4672. doi: 10.1073/pnas.1221400110.
410 17. McMillin M J, Beck A E, Chong J X, Shively K M, Buckingham K J, Gildersleeve H I,
411 Aracena M I, Aylsworth A S, Bitoun P, Carey J C, Clericuzio C L, Crow Y J, Curry C J,
412 Devriendt K, Everman D B, Fryer A, Gibson K, Giovannucci Uzielli M L, Graham J M,
413 Jr., Hall J G et al. 2014. Mutations in PIEZO2 cause Gordon syndrome, Marden-Walker
414 syndrome, and distal arthrogryposis type 5. American journal of human genetics 94;734-
415 744. doi: 10.1016/j.ajhg.2014.03.015.
416 18. Okubo M, Fujita A, Saito Y, Komaki H, Ishiyama A, Takeshita E, Kojima E, Koichihara
417 R, Saito T, Nakagawa E, Sugai K, Yamazaki H, Kusaka K, Tanaka H, Miyake N,
418 Matsumoto N, Sasaki M. 2015. A family of distal arthrogryposis type 5 due to a novel
419 PIEZO2 mutation. American journal of medical genetics. Part A 167A;1100-1106. doi:
420 10.1002/ajmg.a.36881.
421 19. Alisch F, Weichert A, Kalache K, Paradiso V, Longardt A C, Dame C, Hoffmann K,
422 Horn D. 2016. Familial Gordon syndrome associated with a PIEZO2 mutation. American
423 journal of medical genetics. Part A doi: 10.1002/ajmg.a.37997.
424 20. Mahmud A A, Nahid N A, Nassif C, Sayeed M S, Ahmed M U, Parveen M, Khalil M I,
425 Islam M M, Nahar Z, Rypens F, Hamdan F F, Rouleau G A, Hasnat A, Michaud J L.
426 2016. Loss of the proprioception and touch sensation channel PIEZO2 in siblings with a
427 progressive form of contractures. Clinical genetics doi: 10.1111/cge.12850.
428 21. Delle Vedove A, Storbeck M, Heller R, Holker I, Hebbar M, Shukla A, Magnusson O,
429 Cirak S, Girisha K M, O'Driscoll M, Loeys B, Wirth B. 2016. Biallelic Loss of
430 Proprioception-Related PIEZO2 Causes Muscular Atrophy with Perinatal Respiratory
431 Distress, Arthrogryposis, and Scoliosis. American journal of human genetics 99;1206-
432 1216. doi: 10.1016/j.ajhg.2016.09.019.
433 22. Haliloglu G, Becker K, Temucin C, Talim B, Kucuksahin N, Pergande M, Motameny S,
434 Nurnberg P, Aydingoz U, Topaloglu H, Cirak S. 2017. Recessive PIEZO2 stop mutation
435 causes distal arthrogryposis with distal muscle weakness, scoliosis and proprioception
436 defects. Journal of human genetics 62;497-501. doi: 10.1038/jhg.2016.153.

bioRxiv preprint doi: https://doi.org/10.1101/169516; this version posted July 28, 2017. The copyright holder for this preprint (which was not certified by peer review) is the author/funder, who has granted bioRxiv a license to display the preprint in perpetuity. It is made available under aCC-BY 4.0 International license.

437 23. Fotiou E, Martin-Almedina S, Simpson M A, Lin S, Gordon K, Brice G, Atton G, Jeffery
438 I, Rees D C, Mignot C, Vogt J, Homfray T, Snyder M P, Rockson S G, Jeffery S,
439 Mortimer P S, Mansour S, Ostergaard P. 2015. Novel mutations in PIEZO1 cause an
440 autosomal recessive generalized lymphatic dysplasia with non-immune hydrops fetalis.
441 Nature communications 6;8085. doi: 10.1038/ncomms9085.
442 24. Nonomura K, Woo S H, Chang R B, Gillich A, Qiu Z, Francisco A G, Ranade S S,
443 Liberles S D, Patapoutian A. 2017. Piezo2 senses airway stretch and mediates lung
444 inflation-induced apnoea. Nature 541;176-181. doi: 10.1038/nature20793.
445 25. Bai T, Li Y, Xia J, Jiang Y, Zhang L, Wang H, Qian W, Song J, Hou X. 2017. Piezo2: A
446 Candidate Biomarker for Visceral Hypersensitivity in Irritable Bowel Syndrome? Journal
447 of neurogastroenterology and motility doi: 10.5056/jnm16114.
448 26. Syeda R, Xu J, Dubin A E, Coste B, Mathur J, Huynh T, Matzen J, Lao J, Tully D C,
449 Engels I H, Petrassi H M, Schumacher A M, Montal M, Bandell M, Patapoutian A. 2015.
450 Chemical activation of the mechanotransduction channel Piezo1. eLife 4doi:
451 10.7554/eLife.07369.
452 27. Coste B, Murthy S E, Mathur J, Schmidt M, Mechioukhi Y, Delmas P, Patapoutian A.
453 2015. Piezo1 ion channel pore properties are dictated by C-terminal region. Nature
454 communications 6;7223. doi: 10.1038/ncomms8223.
455 28. Klotz I M. 1985. Ligand--receptor interactions: facts and fantasies. Quarterly reviews of
456 biophysics 18;227-259. doi.
457 29. Sandtner W, Egwolf B, Khalili-Araghi F, Sanchez-Rodriguez J E, Roux B, Bezanilla F,
458 Holmgren M. 2011. Ouabain binding site in a functioning Na+/K+ ATPase. The Journal
459 of biological chemistry 286;38177-38183. doi: 10.1074/jbc.M111.267682.

460

461

bioRxiv preprint doi: https://doi.org/10.1101/169516; this version posted July 28, 2017. The copyright holder for this preprint (which was not certified by peer review) is the author/funder, who has granted bioRxiv a license to display the preprint in perpetuity. It is made available under aCC-BY 4.0 International license.

462 **Figure Legends**

463 **Fig. 1 A chimeric approach to determine the Yoda1 binding site in mPiezo1. a** mPiezo1
464 cryo-EM structure (PDBID:3JAC). The indicated structural features are highlighted with
465 differential coloring. **b** Yoda1 chemical structure. **c** Generation of C-terminal chimeras with
466 respect to their approximate position in the mPiezo1 topology (coloring is identical to a).
467 Residue numbers are from mPiezo1; mPZ1=mPiezo1, mPZ1=mPiezo2. **d** Relative Ca^{2+}-sensitive
468 fluorescence time course from HEK293T cells transfected with WT mPZ1 (black and magenta
469 traces) or the empty vector pCDNA3 (blue trace). Cells were pre-loaded with Fluo8-AM and
470 incubated with 30µM Yoda1 (blue and black traces) or a control solution (magenta trace) at t =
471 30 s. **e** Relative fluorescence changes from HEK293T cells expressing the indicated C-terminal
472 chimeras (n = 4 for each plot), mPZ1 (magenta, n = 4) or mPZ2 (purple, n = 4) plotted against
473 Yoda1 concentration at t = 60 s. **f** Relative fluorescence changes from HEK293T cells expressing
474 the indicated construct (n = 5 for each plot) or the empty vector pCDNA3 (control, n = 5)
475 following an acute hypotonic shock. For each construct, the fluorescence signal was compared to
476 the control using a Student's t-test. The numbers of the left of the bars above the histograms
477 indicate the t-values for each test. Asterisks indicate standard p-value range: *: $0.01 < p < 0.05$;
478 **: $0.001 < p < 0.01$ and ***: $p < 0.001$. In all panels, error bars = s.e.m.

479

480 **Fig. 2 A minimal mPiezo1 region responsible for Yoda1 binding. a** Generation of internal
481 chimeras in the mPiezo1 1961-2063 region. Filled regions represent mPZ2 sequence; residue
482 numbers are from mPiezo1. **b** Relative fluorescence changes from HEK293 cells expressing the
483 indicated Chimeras (n = 4 for each plot), mPZ1 (magenta, n = 4) or mPZ2 (dark blue, n = 4)
484 plotted against Yoda1 concentration. **c** Relative fluorescence changes from HEK293T cells

bioRxiv preprint doi: https://doi.org/10.1101/169516; this version posted July 28, 2017. The copyright holder for this preprint (which was not certified by peer review) is the author/funder, who has granted bioRxiv a license to display the preprint in perpetuity. It is made available under aCC-BY 4.0 International license.

485 expressing mPZ1 (n = 6), mPZ2 (n = 5) the Ch1961-2063 chimera (n = 6) or the empty vector
486 pCDNA3 (control, n = 6) following an acute hypotonic shock. For each construct, the
487 fluorescence signal was compared to the control using a Student's t-test. The numbers of the left
488 of the bars above the histograms indicate the t-values for each test. Asterisks indicate standard p-
489 value range: *: $0.01 < p < 0.05$; **: $0.001 < p < 0.01$ and ***: $p < 0.001$. **d** Pressure-clamp
490 electrophysiology recordings in the cell-attached configuration for mPZ1 (magenta traces) and
491 the Ch1961-2063 chimera (blue traces). **e** Normalized peak current as a function of the pressure
492 pulse for mPZ1 (magenta squares, n = 3) and Ch1961-2063 (blue circles, n = 3). The traces
493 correspond to a fit using a classical two-state Boltzmann equation (see text). **f** Position of the
494 1961-2063 sub-regions (1961-2004, yellow; 2005-2034, orange and 2035-2063, blue) relative to
495 the mPiezo1 cryo-EM structure (left: top view, right: side view). In all panels, error bars = s.e.m.
496
497 **Fig. 3 Minimal effective Yoda1 binding stoichiometry. a** Fitting of the mPiezo1 Yoda1 dose
498 response (n = 4) with three binding models corresponding to equations (8), (9) and (10) (see text
499 and Table 1 for fitted parameters). **b** Co-expression of WT mPiezo1 subunits (WT) with Yoda1-
500 insensitive Ch1961-2063 chimera subunits (Ch) yields four distinct channel species with
501 predicted relative fraction as a function of the relative amount of WT vs. Ch subunits. **c** Yoda1
502 dose-responses obtained by mixing WT and Ch subunits with the indicated ratios (n= 4 for each
503 plot). The traces are fit obtained with a global fit from equation (12). **d** Observed vs. predicted
504 fraction of contributing hybrid channels having i WT subunit. Each point is the mean values for
505 six concentrations ranging from 2 to 75 μM for the three tested mixtures. The red line
506 corresponds to the linear function $y = x$. In all panels, error bars = s.e.m.
507

bioRxiv preprint doi: https://doi.org/10.1101/169516; this version posted July 28, 2017. The copyright holder for this preprint (which was not certified by peer review) is the author/funder, who has granted bioRxiv a license to display the preprint in perpetuity. It is made available under aCC-BY 4.0 International license.

508 **Video1: Wide-field live-cell fluorescence imaging showing Yoda1-mediated Piezo1**
509 **activation**. HEK293T cells co-expressing GCaMP6m and mPiezo1 were exposed to 100 µM
510 Yoda1 at t = 10 sec. Individual images showing GCaMP6m fluorescence were acquired at 1
511 frame/ sec and displayed in the movie at 5 frames/sec.
512
513 **Video2: Piezo1-dependent Yoda1-induced GCaMP6m fluorescence changes.** HEK293T cells
514 expressing GCaMP6m only were exposed to 100 µM Yoda1 at t = 10 sec. Individual images
515 showing GCaMP6m fluorescence were acquired at 1 frame/ sec and displayed in the movie at 5
516 frames/sec.
517
518 **Supplementary Figure 1: Sequence alignment (T-coffee) of the C-terminal region of mouse**
519 **Piezo1 (mPZ1), Piezo2 (mPZ2) and human Piezo1 (hPZ1) and Piezo2 (hPZ2).** The residues
520 numbers correspond to positions used to create the chimeras. Asterisks indicate residues within
521 the 1961-2063 region that are not conserved between mPiezo1 and mPiezo2.

a

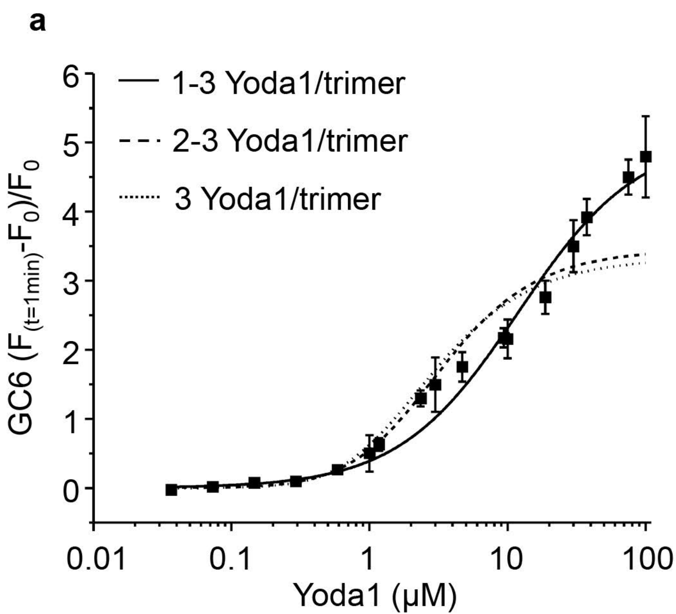

b

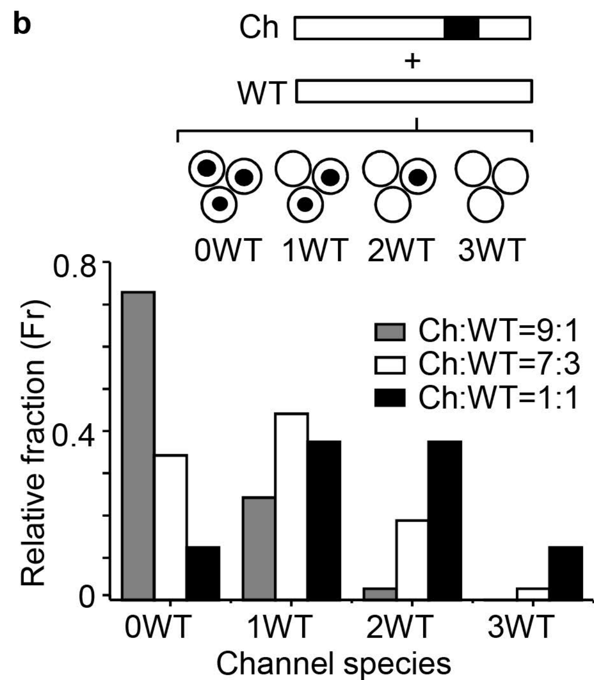

c

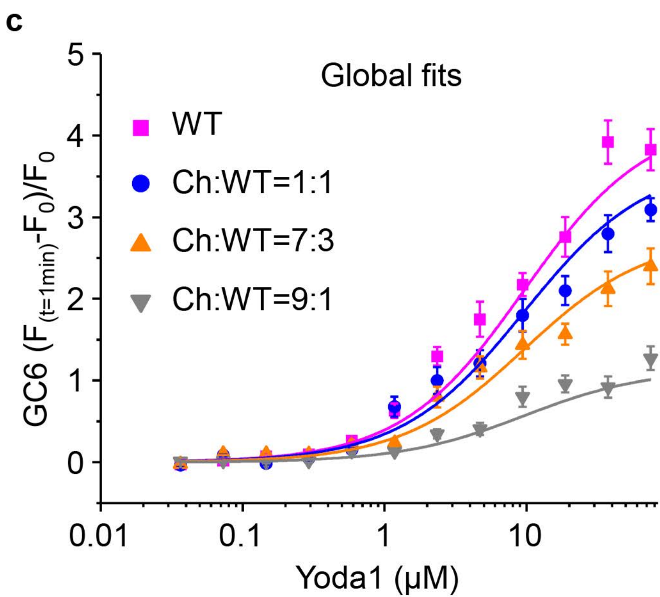

d

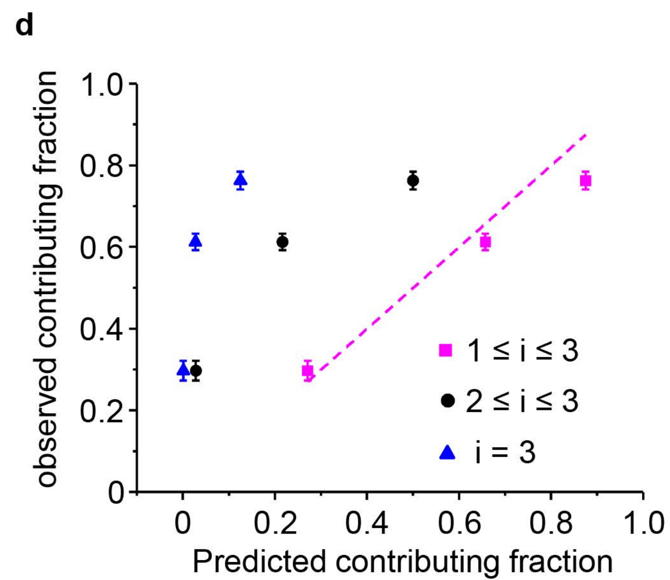

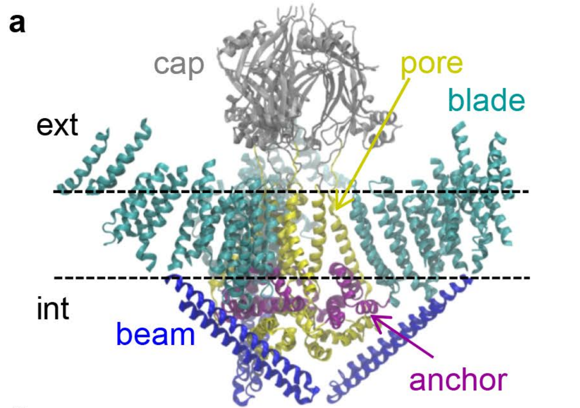
a
cap
pore
blade
ext
int
beam
anchor

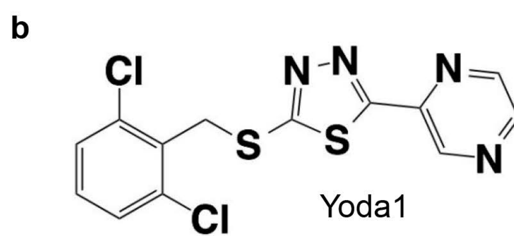
b
Cl
N
N
N
S
S
N
Cl
Yoda1

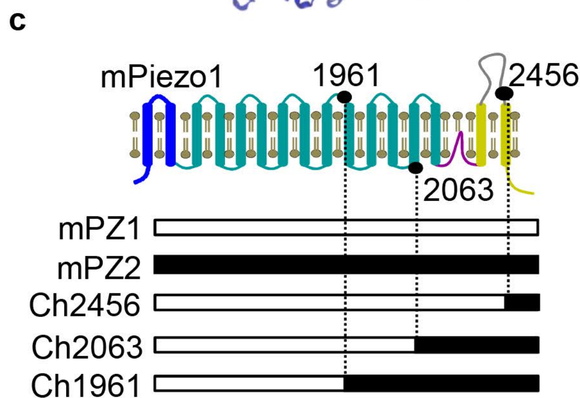
c
mPiezo1
1961
2456
2063
mPZ1
mPZ2
Ch2456
Ch2063
Ch1961

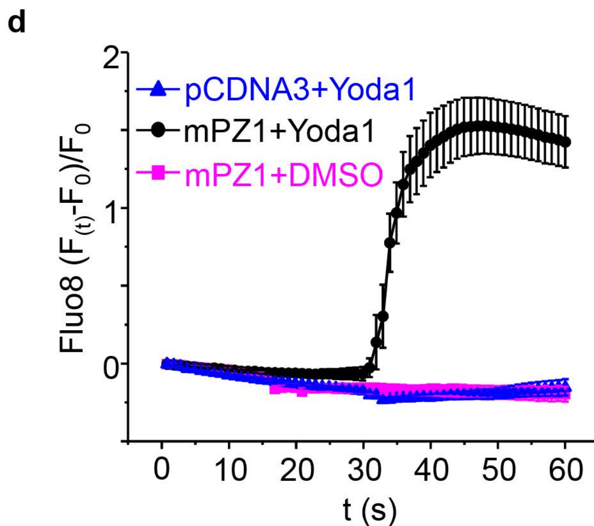
d
pCDNA3+Yoda1
mPZ1+Yoda1
mPZ1+DMSO
Fluo8 (F(t)-F0)/F0
t (s)

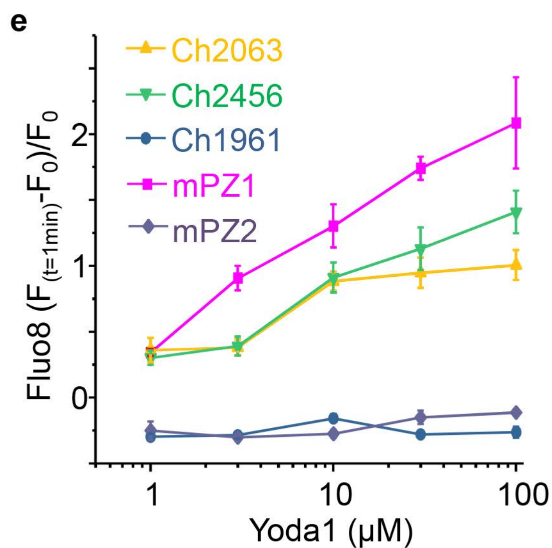
e
Ch2063
Ch2456
Ch1961
mPZ1
mPZ2
Fluo8 (F(t=1min)-F0)/F0
Yoda1 (μM)

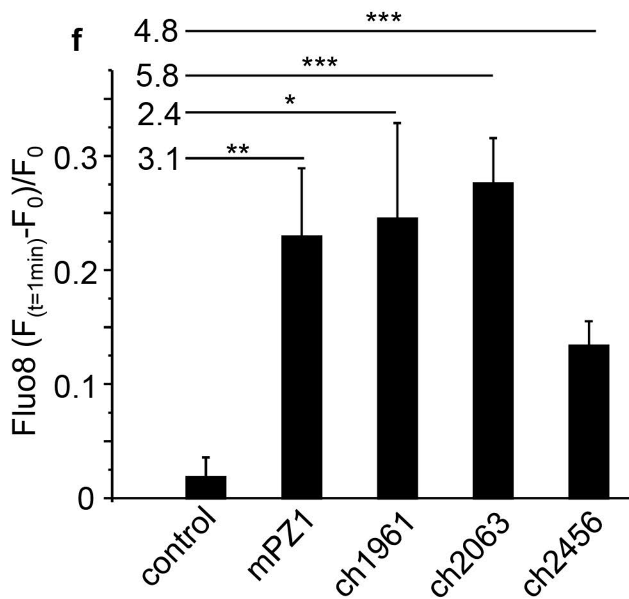
f
4.8
5.8
2.4
3.1
***
***
*
**
Fluo8 (F(t=1min)-F0)/F0
control
mPZ1
ch1961
ch2063
ch2456

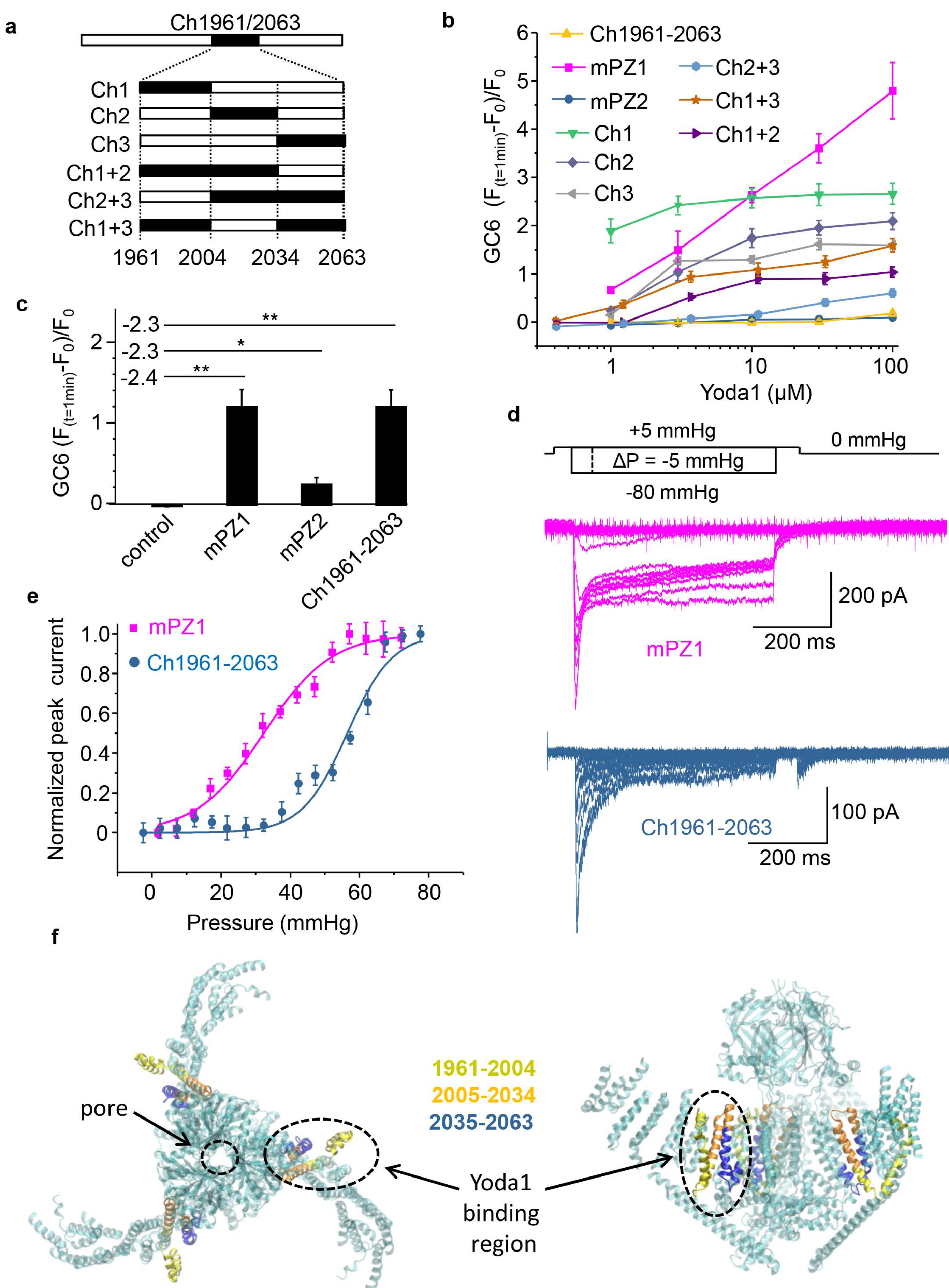
a
Ch1961/2063
Ch1
Ch2
Ch3
Ch1+2
Ch2+3
Ch1+3
1961
2004
2034
2063
b
Ch1961-2063
mPZ1
Ch2+3
mPZ2
Ch1+3
Ch1
Ch1+2
Ch2
Ch3
GC6 (F(t=1min)-F0)/F0
Yoda1 (µM)
c
-2.3
-2.3
-2.4
**
*
**
GC6 (F(t=1min)-F0)/F0
control
mPZ1
mPZ2
Ch1961-2063
d
+5 mmHg
0 mmHg
ΔP = -5 mmHg
-80 mmHg
200 pA
200 ms
mPZ1
100 pA
Ch1961-2063
200 ms
e
mPZ1
Ch1961-2063
Normalized peak current
Pressure (mmHg)
f
pore
1961-2004
2005-2034
2035-2063
Yoda1
binding
region